Adsorption 11: 289–294, 2005

Temperature Effect on Adsorption/Desorption Isotherms for a Simple Fluid Confined within Various Nanopores

BENOÎT COASNE AND KEITH E. GUBBINS
Department of Chemical and Biomolecular Engineering, 113 Riddick Labs, North Carolina St. Univ., Raleigh, NC 27695, USA

ROLAND J.-M. PELLENQ*
Centre de Recherche de la Matière Condensée et des Nanosciences CRMC-N, UPR – CNRS 7251, Campus de Luminy, 13288 Marseille Cedex 09, France
pellenq@crmcn.univ-mrs.fr

Abstract. We report a Grand Canonical Monte Carlo study of the temperature dependence of adsorption/desorption hysteresis for porous matrices having different morphologies and topologies. We aim at gaining some insights on the concept of critical hysteresis temperature, T_{cc}, defined as the temperature at which the hysteresis loop disappears. Simulated T_{cc} for cylindrical, ellipsoidal, and constricted pores follow the experimental scaling law established for MCM-41 silica materials. In contrast, T_{cc} for Vycor samples with a largest pore size $\sim$2.5 nm and 5.0 nm obey a different relationship, in qualitative agreement with experiments.

Keywords: capillary condensation, Monte-Carlo simulation, nanoporous material, hysteresis

1. Introduction

Nanoporous materials are made either of connected or unconnected pores. Materials with independent pores include solids such as etched track porous silicon, carbon nanotubes, MCM-41, and SBA-15 silicas. Networked porous solids are usually glasses such as Vycor or CPG materials (Gelb et al., 1999). Condensation and freezing phenomena of molecular fluids are routinely used for characterization purpose using macroscopic physical laws such as the well know Kelvin or Gibbs-Thompson equations, which link a thermodynamic quantity to the mean pore size (Neimark et al., 2003). These approaches implicitly assume (i) that such phenomena are first order transitions involving gas/liquid or liquid/solid phase coexistences, and (ii) that interfacial properties can be described by some physical quantities such as surface tensions. Adsorption/desorption isotherm (adsorbed amount *versus* pressure) is a standard measure of the capillary condensation phenomenon: it usually presents a characteristic hysteresis loop that shrinks and disappears as the temperature increases. This is observed for all nanoporous materials made of independent unconnected pores or exhibiting a connected pore network. In this work, we do not consider microporous materials such as zeolites (with pores less than 1.5 nm in diameter) that are systems that can be defined by the absence of capillary phenomena. In the case of connected pores, such a hysteretic behavior is usually interpreted as the consequence of the existence of constrictions between the pores. On the other hand, the hysteresis loop observed for unconnected regular pores is explained as the consequence of a change in the symmetry of the liquid/gas interface during the filling and emptying processes (Gelb et al., 1999). Density Functional or Lattice Gas theories have shown that the first order character of fluid condensation is relevant for unconnected slit pores only. Indeed, no first order transition can occur in a cylindrical pore since such geometry is viewed

*To whom correspondence should be addressed.

as a quasi-one dimensional system (Evans, 1990). In the case of disordered and connected porous networks, recent lattice-gas calculations have shown that capillary condensation cannot be considered either as a true first-order transition; the disorder generates a complex free energy landscape, with a huge number of local minima (i.e. metastable states), in which the system remains trapped without finding the true equilibrium state (Detcheverry et al., 2004). Therefore, the present state of the art for capillary condensation in nanoporous systems distinguishes materials with unconnected slit pores and networked pores. There seems to be some experimental support for this separation (Fig. 1): depending on the type of porous structures, the hysteresis critical temperature, T_{cc}, at which the hysteresis loop disappears, obeys two different laws with respect to the pore size (reduced by the adsorbate size). The status of this hysteresis critical temperature as being or not relevant to a true critical point in the context of disordered mesoporous systems, is not clear and beyond the scope of the present study. We note that Woo and Monson (2003) performing *on-lattice* mean field and Monte-Carlo simulations in the case of vycor, indicate the existence of a true first-order transition with a critical point that occurs at lower temperature than T_{cc}. However, the mapping of these on-lattice results onto more realistic atomic-scale situations attainable with atomistic off-lattice techniques (Gelb et al., 2002; Pellenq et al., 2002) remains difficult (in particular concerning the dependence of on-lattice results with the lattice spacing and the absolute value of the so-called y parameter that is defined as the ratio of the on-lattice surface-fluid to the fluid-fluid energy parameters).

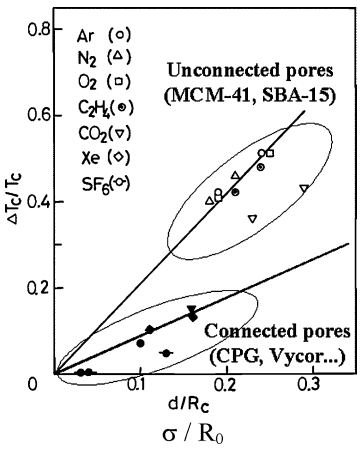

Figure 1. Experimental hysteresis critical temperature as a function of the mean pore size, R_0, and the adsorbate molecule diameter (σ). T_c is the bulk critical temperature and $\Delta T_c = T_c - T_{cc}$ (adapted from Morishige et al., 1997). Two linear laws are observed, depending on the type of porous structures: unconnected or connected pores.

In this work, we report Grand Canonical Monte Carlo (GCMC) simulations of condensation of a simple molecular fluid, Ar, in connected and independent silica nanopores. We also explore the effect of the pore shape by considering pores of various sections. We aim at gaining some insights on the concept of hysteresis critical temperature and its dependence on the pore morphology and topology.

2. Computational Techniques

The GCMC technique consists of determining the properties of a system at a constant volume V (the pore with the adsorbed phase) in equilibrium with an infinite fictitious reservoir of particles imposing its chemical potential μ and its temperature T (Frenkel and Smit, 2002). Pores used in our simulations were prepared from a cube of non porous silica cristoballite. This allows cutting out portions of this initial volume in order to obtain different porous matrices. In order to model the pore inner surface in a realistic way, we removed all silicon atoms being in an incomplete tetrahedral environment and all non-bonded oxygen atoms. The electroneutrality of the simulation box is ensured by saturating all oxygen dangling bonds with hydrogen atoms; the partial charges carried by the atoms of the substrate are $q_O = -1e$, $q_{Si} = +2e$ and $q_H = +0.5e$. Regular or irregular cylindrical pores can be easily prepared with this procedure: pores are defined by simple mathematical functions. In contrast, the case of disordered porous solids needs an important effort to produce 3D numerical matrices and account for the morphology and topology of the real material Vycor. The sample studied in this paper was obtained by an off-lattice reconstruction method described elsewhere (Pellenq and Levitz, 2002) that we applied to a 7.13^3 nm^3 box of silica cristoballite: the resulting structure has a mean pore dimension of 1.8 nm and a largest cavity of 2.5 nm. Interactions between the different adsorbates and substrate atoms were calculated using the PN-TraZ potential, which was initially developed for rare gas adsorption in zeolite (Pellenq and Nicholson, 1994). This intermolecular potential function has been used to model successfully the adsorption of water on silica glasses (Puibasset and Pellenq, 2003). In order to accelerate GCMC simulation runs, we calculated the adsorbate/substrate interaction using an energy grid,

which splits the simulation box volume into a collection of voxells (about 1 Å^3). The adsorbate/substrate energy is then obtained by interpolating the 3D energy grid. The Ar/Ar interaction was calculated using a Lennard-Jones potential ($\varepsilon = 120$ K and $\sigma = 0.34$ nm). The bulk saturating vapor pressure P_0 of Ar was determined from the parameters of the Lennard-Jones potential according to the equation of state by Kofke (1993). Full details of the simulation method have been given elsewhere (Coasne and Pellenq, 2004a).

3. Results

3.1. Cylindrical Pore Geometry

Adsorption/desorption isotherms for a 3.6 nm cylindrical pore are shown in Fig. 2(a). $T_{cc} = 94.5$ K was estimated as the average value between the largest value of temperature, $T = 93$ K, for which a hysteresis loop is observed and that, $T = 96$ K, of the next (reversible) isotherm. We note that the given pore size 3.6 nm is that used in the numerical process for generating the pore. The actual size 3.1 nm is somewhat smaller, due to the hydrogen atoms at the surface of the pore. This correction is needed when comparing our data to other simulation works based on smooth structure-less walls (see below) or to disordered systems since their pore size distribution is known by probing the adsorbate accessible volume. We have considered several cylindrical pores with radius R_0 (nm) $= \{1.4, 1.8, 2.5, 2.8\}$; the corresponding hysteresis critical temperatures are T_{cc}((K) $= \{85, 94, 112, 115\}$, respectively. In this work, the desorption branch necessarily corresponds to a cavitation (metastable) process since pores are of a infinite length. It has been shown that the desorption occurs at equilibrium, provided the confined fluid is in direct contact with the gas reservoir through an interface (Coasne, 2003). However this has a negligible effect since in both cases (infinite and finite pores) the hysteresis loops closes and disappears almost at the same temperature (Gelb, 2002).

3.2. Ellipsoidal Pore Geometry

Figure 2(b) shows Ar adsorption isotherms in a 5.0 × 2.5 nm ellipsoidal silica pore at different temperatures. The hysteresis critical temperature for this pore was obtained as for the cylindrical pores (see Fig. 2(a)). T_{cc} for the ellipsoidal pore having an average size of 3.6 nm was found identical to that for the 3.6 nm cylinder, $T_{cc} = 94.5$ K.

3.3. Cylindrical Pore with a Constriction

In Fig. 3, we present equilibrium snapshots along the Ar adsorption/condensation process in a 5.0 nm cylindrical silica pore with a 2.5 nm constriction. Again, the average pore size is 3.6 nm. In Fig. 4(a), we show the Ar adsorption/desorption isotherms for this pore at different temperatures. The hysteresis critical temperature for this system is 108 K, which is significantly higher

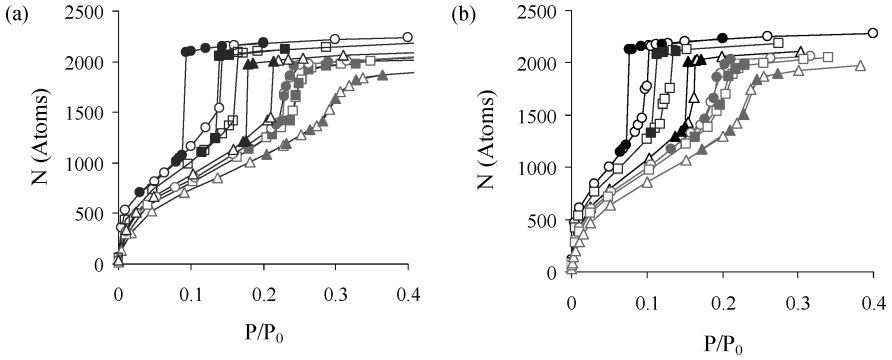

Figure 2. (a) Ar adsorption isotherms in a 3.6 nm cylindrical silica pore at different temperatures. Black and gray data correspond to temperatures below and above the hysteresis critical temperature of the confined fluid, respectively: (black circles) $T = 77$ K, (black squares) $T = 83$ K, (black triangles) $T = 93$ K, (gray circles) $T = 96$ K, (gray squares) $T = 99$ K and (gray triangles) $T = 110$ K. Open and closed symbols are adsorption and desorption data, respectively. (b) Ar adsorption isotherms in a 5.0 × 2.5 nm ellipsoidal silica pore at different temperatures. Black and gray data correspond to temperatures below and above the hysteresis critical temperature of the confined fluid, respectively: (black circles) $T = 77$ K, (black squares) $T = 83$ K, (black triangles) $T = 93$ K, (gray circles) $T = 96$ K, (gray squares) $T = 99$ K and (gray triangles) $T = 110$ K. Open and closed symbols are adsorption and desorption data, respectively.

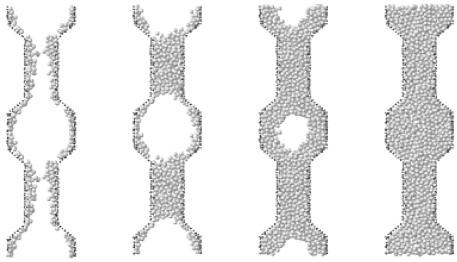

Figure 3. Configurations of Ar atoms adsorbed at $T = 77$ K in a 5.0 nm cylindrical silica pore with a 2.5 nm constriction: (a) at (a) $P = 0.04\ P_0$, (b) $P = 0.08\ P_0$, (c) $P = 0.25\ P_0$ and (d) $P = 0.26\ P_0$. Black dots correspond to the hydrogen atoms, which delimitate the pore surface and the light colored spheres are Ar atoms. (From Coasne et al., 2004).

than that for the 3.6 nm cylindrical pore, $T_{cc} = 94.5$ K. However, the analysis of the equilibrium snapshots shows that the final condensation and the onset of the evaporation process are located in the largest cavity having a size of 5 nm. Consequently, the hysteretic critical temperature for the constricted pore is close to that obtained for a 5 nm cylindrical regular pore, $T_{cc} = 112$ K.

3.4. Disordered Porous Matrix

In Fig. 4(b), we show a set of Ar adsorption isotherms for a "small" Vycor sample. In this case, $T_{cc} = 85$ K was estimated as the intercept of the straight lines [$\ln(P_{ADS}/P_0)$ and $\ln(P_{DES}/P_0)$ vs. $1/T$], (see insert in Fig. 4(b)) (Pellenq and Levitz, 2002). As already shown (Pellenq et al., 2001; Gelb and Gubbins, 1999; Kierlik et al., 2001; Woo et al., 2001), the pore disorder changes the overall shape of the adsorption/desorption isotherms compared to that for regular cylindrical pores. Interestingly, the adsorption isotherms for Vycor resemble those obtained for the constricted pore. A detailed comparison between the adsorption/desorption behaviors observed for both pore morphologies/topologies can be found in references (Coasne et al., 2004; Coasne and Pellenq, 2004b).

4. Discussion and Conclusion

We now discuss the effect of the pore morphology (cylindrical, ellipsoidal, and constricted pores) and topology (Vycor porous glasses) on the temperature dependence of capillary condensation hysteresis in nanoporous materials. In Fig. 5, we plot the relative decrease of the hysteresis critical temperature, T_{cc}, with respect to the bulk critical temperature, T_c, as a function of the pore size R_0 (reduced to the size of the adsorbate molecule taken as the tabulated kinetic diameter σ). We also report data taken from the literature for xenon, $\sigma = 0.39$ nm, in a Vycor-like sample having a largest cavity of 5 nm (Gelb and Gubbins, 2002), and for water, $\sigma = 0.28$ nm, in a cylindrical pore of a diameter 2.4 nm (Brovchenko et al., 2004). The first important result in this work is the ability of GCMC simulations to reproduce correctly the experimental behavior $\Delta T_{cc}/T_c = 2\sigma/R_0$ for small independent nanopores ($R_0 < 5.0$ nm). We note that this scaling law seems to be independent of the nature of the adsorbate since both water data (Brovchenko et al.,

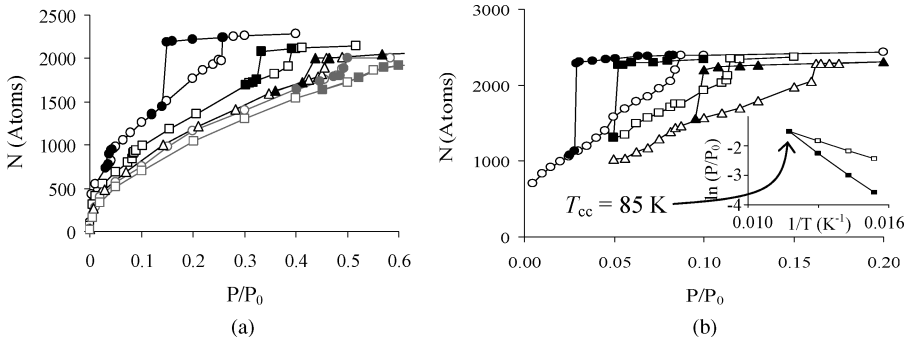

Figure 4. (a) Ar adsorption isotherms in a 5.0 nm cylindrical silica pore with a 2.5 nm constriction at different temperatures. Black and gray data correspond to temperatures below and above the hysteresis critical temperature of the confined fluid, respectively: (black circles) $T = 77$ K, (black squares) $T = 93$ K, (black triangles) $T = 105$ K, (gray circles) $T = 110$ K, (gray squares) $T = 120$ K. Open and closed symbols are adsorption and desorption data, respectively. (b) Ar adsorption isotherms in a Vycor silica porous material with a largest cavity of 2.5 nm for different temperatures: (black circles) $T = 65$ K, (black squares) $T = 70$ K, (black triangles) $T = 77$ K. Open and closed symbols are adsorption and desorption data, respectively. Insert: Estimate of T_{cc} from the intercept of the straight lines [$\ln(P_{ADS}/P_0)$ and $\ln(P_{DES}/P_0)$ vs. $1/T$] (see text).

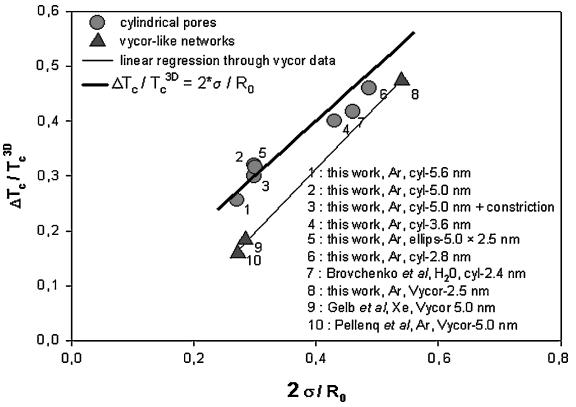

Figure 5. Hysteresis critical temperature as a function of the mean pore size, R_0, and the adsorbate molecule diameter (σ). T_c is the bulk critical temperature and $\Delta T_c = T_c - T_{cc}$ (see text).

2004) and our Ar data for argon fall on this master curve. In contrast, T_{cc} for Vycor samples do not seem to obey this scaling law. Indeed, Vycor data for both argon (this work and Pellenq et al., 2001) and xenon (Gelb and Gubbins, 2002) fall on a straight line that departs from that observed for the simple geometries. Interestingly, such an effect of the pore topology in the case of large pores is also observed in the experiment (see data for materials with connected pores in Fig. 1). The reasons for such a behavior in the case of Vycor samples with large cavities is not clear yet. This can be interpreted as a strong effect of the pore disorder. Further investigation is required to clarify this issue.

Acknowledgments

This work was supported in part by the National Science Foundation through grants no. CTS-0211792 and INT–0089696 and in part by the Petroleum Research Fund of the American Chemical Society. Supercomputing time was provided by the National Partnership for Advanced Computational Infrastructure (NPACI-NPA 205) and the Institut de Développement et des Ressources en Informatique Scientifique (IDRIS, CNRS).

References

Brovchenko, I., A. Geiger, and A. Oleinikova, "Water in Nanopores. I. Coexistence Curves From Gibbs Ensemble Monte Carlo Simulations," *J. Chem. Phys.*, **120**, 1958–1972 (2004).

Coasne, B., "Adsorption et Condensation de Fluides Simples dans le Silicium Mésoporeux: Une Approche Expérimentale et par Simulation Monte Carlo," Ph.D. Thesis, University, Paris 7, France, 2003.

Coasne, B., K.E. Gubbins, and R.J.-M. Pellenq, "A Grand Canonical Monte Carlo Study of Adsorption and Capillary Phenomena in Nanopores of Various Morphologies and Topologies: Testing the BET and BJH Characterization Methods," *Part. Part. Char. Syst.*, **21**, 149–160 (2004).

Coasne, B. and R.J.-M. Pellenq, "Grand Canonical Monte Carlo Simulation of Argon Adsorption at the Surface of Silica Nanopores: Effect of Pore Size, Pore Morphology, and Surface Roughness," *J. Chem. Phys.*, **120**, 2913–2922 (2004a).

Coasne, B. and R.J.-M. Pellenq, "A Grand Canonical Monte Carlo Study of Capillary Condensation in Mesoporous Media: Effect of the Pore Morphology and Topology," *J. Chem. Phys.*, **121**, 3767–3774 (2004b).

Detcheverry, F. et al., "Hysteresis in Capillary Condensation of Gases in Disordered Porous Solids," *Physica B*, **343**, 303–307 (2004).

Evans, R., "Fluids Adsorbed in Narrow Pores: Phase Equilibria and Structure," *J. Phys.: Condens. Matter.*, **2**, 8989–9007 (1990).

Frenkel, D. and B. Smit, *Understanding Molecular Simulation*, 2nd ed., New York, Academic, New York, 2002.

Gelb, L.D., "The Ins and Outs of Capillary Condensation in Cylindrical Pores," *Mol. Phys.*, **100**, 2049–2057 (2002).

Gelb, L.D. and K.E. Gubbins, "Pore Size Distribution in Porous Glasses: A Computer Simulation Study," *Langmuir*, **15**, 305–308 (1999).

Gelb, L.D. and K.E. Gubbins, "Molecular Simulation of Capillary Phenomena in Controlled Pore Glasses," *Fundamentals of Adsorption* **7**, 333–340 (2002).

Gelb, L.D., K.E. Gubbins, R. Radhakrishnan, and M. Sliwinska-Bartkowiak, "Phase Separation in Confined Systems," *Rev. Prog. Phys.*, **62**, 1573–1659 (1999).

Kierlik, E., P.A. Monson, M.L. Rosinberg, L. Sarkisov, and G. Tarjus, "Capillary Condensation in Disordered Porous Materials: Hysteresis versus Equilibrium Behavior," *Phys. Rev. Lett.*, **87**, 055701 (2001).

Kofke, D.A., "Direct Evaluation of Phase Coexistence by Molecular Simulation *via* Integration Along the Saturation Line," *J. Chem. Phys.*, **98**, 4149–4162 (1993).

Morishige, K., H. Fujii, M. Uga, and D. Kinukawa, "Capillary Critical Point of Argon, Nitrogen, Oxygen, Ethylene and Carbon Dioxide in MCM-41," *Langmuir*, **13**, 3494–3498 (1997).

Neimark, A.V., P.I. Ravikovitch, and A. Vishnyakov, "Bridging Scales From Molecular Simulations to Classical Thermodynamics: Density Functional Theory of Capillary Condensation in Nanopores," *J. Phys.: Condens. Matter*, **15**, 347–365 (2003).

Pellenq, R.J.-M. and P.E. Levitz, "Capillary Condensation in a Disordered Mesoporous Medium: A Grand Canonical Monte Carlo Study," *Mol. Phys.*, **100**, 2059–2077 (2002).

Pellenq, R.J.-M. and D. Nicholson, "Intermolecular Potential Function for the Physical Adsorption of Rare Gases in Zeolite," *J. Phys. Chem.*, **98**, 13339–13349 (1994).

Pellenq, R.J.-M., B. Rousseau, and P.E. Levitz, "A Grand Canonical Monte Carlo Study of Argon Adsorption/Condensation in Mesoporous Silica Glasses," *Phys. Chem. Chem. Phys.*, **3**, 1207–1212 (2001).

Puibasset, J. and R.J.-M. Pellenq, "Grand Canonical Monte Carlo Study of Water Structure on Hydrophilic Mesoporous and Plane Silica Substrates," *J. Chem. Phys.*, **119**, 9226–9232 (2003).

Woo, H.J., L. Sarkisov, and P.A. Monson, "Mean Field Theory of Fluid Adsorption in a Porous Glass," *Langmuir*, **17**, 7472–7475 (2001).

Woo, H.J. and Monson P.A., "Phase Behavior and Dynamics of Fluids in Mesoporous Glasses," *Phys. Rev. E*, **67**, 041207, 1–17 (2003).